CrossMark

Uncertainties in historical changes and future projections of drought. Part II: model-simulated historical and future drought changes

Tianbao Zhao[1] · Aiguo Dai[2,3]

© Springer Science+Business Media Dordrecht 2016

Abstract While most models project large increases in agricultural drought frequency and severity in the 21st century, significant uncertainties exist in these projections. Here, we compare the model-simulated changes with observation-based estimates since 1900 and examine model projections from both the Coupled Model Inter-comparison Project Phase 3 (CMIP3) and Phase 5 (CMIP5). We use the self-calibrated Palmer Drought Severity Index with the Penman-Monteith potential evapotranspiration (PET) (sc_PDSI_pm) as a measure of agricultural drought. Results show that estimated long-term changes in global and hemispheric drought areas from 1900 to 2014 are consistent with the CMIP3 and CMIP5 model-simulated response to historical greenhouse gases and other external forcing, with the short-term variations within the model spread of internal variability, despite that regional changes are still dominated by internal variability. Both the CMIP3 and CMIP5 models project continued increases (by 50–200 % in a relative sense) in the 21st century in global agricultural drought frequency and area even under low-moderate emissions scenarios, resulting from a decrease in the mean and flattening of the probability distribution functions (PDFs) of the sc_PDSI_pm. This flattening is especially pronounced over the Northern Hemisphere land, leading to increased drought frequency even over areas with increasing sc_PDSI_pm. Large differences exist in the CMIP3 and CMIP5 model-projected precipitation and drought changes over the

---

This article is part of a Special Issue on "Decadal Scale Drought in Arid Regions" edited by Zong-Liang Yang and Zhuguo Ma.

✉ Tianbao Zhao
zhaotb@tea.ac.cn

✉ Aiguo Dai
adai@albany.edu

[1] Key Laboratory of Regional Climate-Environment Research for East Asia, Institute of Atmospheric Physics (IAP), Chinese Academy of Sciences (CAS), Beijing, China

[2] Department of Atmospheric and Environmental Sciences, University at Albany, SUNY, Albany, NY, USA

[3] National Center for Atmospheric Research, Boulder, CO, USA

⌔ Springer

Sahel and northern Australia due to uncertainties in simulating the African Inter-tropical convergence zone (ITCZ) and the subsidence zone over northern Australia, while the wetting trend over East Africa reflects a robust response of the Indian Ocean ITCZ seen in both the CMIP3 and CMIP5 models. While warming-induced PET increases over all latitudes and precipitation decreases over subtropical land are responsible for mean sc_PDSI_pm decreases, the exact cause of its PDF flattening needs further investigation.

1 Introduction

Many studies have shown that drought, mainly agricultural drought, may become more severe and widespread under greenhouse gas (GHG)-induced global warming in the 21st century based on model projections (Rind et al. 1990; Wang 2005; Burke et al. 2006; Burke and Brown 2008; Sheffield and Wood 2008; Dai 2011a, 2013a; Wehner et al. 2011; Taylor et al. 2013; Cook et al. 2014; Prudhomme et al. 2014; Zhao and Dai 2015). For the American Southwest and Central Plains, the projected drying is unprecedented for the last 1000 years (Cook et al. 2015). There are still large uncertainties, however, in recent and projected future drought changes, especially regarding the extent to which the drought trends will be forced by changes in precipitation versus evaporative demand (Hobbins et al. 2008; Sheffield et al. 2012; Taylor et al. 2013; Trenberth et al. 2014). In part I of this study (Dai and Zhao 2016), we examined the main uncertainty sources in current estimates of historical drought trends and concluded that surface warming since 1980 has enhanced the drying trend over global land areas.

Model-projected drought changes depend on drought indices and future emissions scenarios analyzed (Burke and Brown 2008; Taylor et al. 2013). The Palmer Drought Severity Index (PDSI; Palmer 1965), a measure of agricultural drought, and its variants (Dai 2011a) are one of the popular drought indices that have been used to quantify past and future aridity and drought changes around the world (Dai et al. 1998, 2004; Dai 2011a, b, 2013a; van der Schrier et al. 2007, 2011, 2013; Sheffield et al. 2012; Zhai et al. 2010; Cook et al. 2014, 2015; Zhao and Dai 2015). However, the original PDSI overestimates the drying trend associated with rising temperatures because of its use of the simple Thornthwaite equation for the potential evapotranspiration (PET) (Burke et al. 2006; Hobbins et al. 2008; Dai 2011b; van der Schrier et al. 2011). To overcome this problem, most applications of the PDSI to future climates used the Penman-Monteith equation for estimating PET (Burke et al. 2006; Burke and Brown 2008; Dai 2011a, b; Taylor et al. 2013; Cook et al. 2014, 2015; Zhao and Dai 2015). Zhao and Dai (2015) showed that the relationship between the self-calibrated PDSI (Wells et al. 2004) with the Penman-Monteith PET (sc_PDSI_pm) and soil moisture content or runoff is similar during the current and future climates in model simulations from the Coupled Model Intercomparison Project phase 5 (CMIP5; Taylor et al. 2012); they also showed that the change patterns in these different drought indices are comparable in CMIP5 model projections although the magnitude of change varies among the indices.

Besides the uncertainties associated with the emissions scenario and indices analyzed, it is unclear whether the drought projections change significantly from the Coupled Model Intercomparison Project phase 3 (CMIP3, Meehl et al. 2007) to phase 5 (CMIP5; Taylor et al. 2012). Some improvements have been noticed from the CMIP3 to CMIP5 models (IPCC 2013), including a larger number of modeling centers and models, the use of moderately higher resolution, and the inclusion of more complex and complete representation of Earth

system processes. However, it is unclear whether the CMIP5 models have improved over the CMIP3 models in terms of simulating historical drought changes, and whether their future projections are comparable. Besides Dai (2013a), who briefly compared historical drought changes from CMIP5 models and observational estimates, there have been few studies that examine drought changes in historical model simulations.

In this paper, we further assess the historical drought changes simulated by both generations of the CMIP models by comparing with the observation-based sc_PDSI_pm, and then compare the drought changes projected by the CMIP3 and CMIP5 models. These comparisons will reveal the agreements and disagreements between the projections by the two generations of models, thereby helping us understand the robustness and uncertainties in model projected drought changes. In the following, we firstly describe the data and method in Section 2. The simulated historical drought changes and their leading modes are evaluated against the observation-based sc_PDSI_pm in Section 3. In Section 4, the CMIP3 and CMIP5 model-simulated future drought changes are described. A summary is given in Section 5.

2 Data and method

The observation-based monthly sc_PDSI_pm used here is described in part I of this study (Dai and Zhao 2016). It was calculated using the merged precipitation dataset (referred to as DaiP) and other updated forcing data on a 2.5° grid from 1850 to 2014. Model sc_PDSI_pm was first calculated using the output from each of the 12 CMIP3 models (Dai 2013a) and 14 CMIP5 models (Zhao and Dai 2015) (Table 1, one ensemble simulation for each model), and then the sc_PDSI_pm values for individual models were simply averaged over the models to create the multi-model ensemble mean for the CMIP3 and CMIP5 models. The all-forcing historical simulations from 1900 to the early 21st century (2000 and 2005 for the CMIP3 and the CMIP5, respectively) and the 21st century simulations under a moderate (A1B) emissions scenarios for the CMIP3 and a low-moderate (RCP4.5) scenario for the CMIP5 were used in this study. As the A1B is a slightly higher emissions scenario than the RCP4.5 after about 2060s, it is expected that the CMIP3 models may produce slightly larger changes. However, we should expect similar change patterns if the model-simulated changes are robust signals.

All the model data were re-mapped onto a common 2.5°lat × 2.5°lon grid, from which the sc_PDSI_pm was calculated. As in all our previous studies, we used 1950–1979 as the calibration period in all the sc_PDSI_pm calculations for reasons discussed in part I of this study. Because the observation-based data are unavailable over many land areas before about 1950, the evaluation for the model simulations focuses on the periods from 1950 to 2014 over global land areas from 60° S-60° N. Besides examining global maps and global averages, regional averages are also examined for five selected areas defined as: Southeast Asia (21.25°–36. 25° N, 101.25°–121.25° E), the western United States (33.75°–46.25° N, 121.25°–103.75° W), Europe (38.75°–51.25° N, 11.25° W–23.75° E), Southeast Australia (23.75°–38.75° S, 138.75°–153.75° E), and southern Africa (33.75°–21.25° S, 13.75°–23.75° E). The linear trend of the sc_PDSI_pm was estimated using the robust-fit method, which considers the effects of outliers and end points (Street et al. 1988; see http://cn.mathworks.com/help/stats/robustfit.html). To explain the sc_PDSI_pm changes, precipitation (P) changes are also discussed.

The mean and variance of the sc_PDSI_pm should be similar to those of the original PDSI over the central U.S., thus Palmer (1965)'s thresholds for various types of drought can still be

Table 1 A list of the CMIP3 and CMIP5 models used in this study

Model center	CMIP3	CMIP5
Bjerknes Centre for Climate Research, Norway	BCCR-BCM2.0	
Canadian Centre for Climate Modelling and Analysis, Canada	CGCM3.1	CanESM2
Canadian Centre for Climate Modelling and Analysis, Canada	CGCM3.1-t63	
National Center for Atmospheric Research (NCAR), USA		CCSM4
Centre National de Recherches Meteorologiques/Centre Europeen de Recherche et Formation Avancees en Calcul Scientifique, France	CNRM-CM3	CNRM-CM5
Commonwealth Scientific and Industrial Research Organisation in collaboration with the Queensland Climate Change Centre of Excellence, Australia	CSIRO-MK3.5	CSIRO-MK3-6-0
LASG, Institute of Atmospheric Physics, Chinese Academy of Sciences	FGOALSg1.0	
NASA Goddard Institute for Space Studies, USA	GISS-AMO	GISS-E2-R
Met Office Hadley Centre, UK		HadGEM2-CC
Met Office Hadley Centre, UK		HadGEM2-ES
Institute for Numerical Mathematics, Russia	INM-CM3.0	INM-CM4
Institute Pierre-Simon Laplace, France	IPSL-CM4	IPSL-CM5A-LR
Japan Agency for Marine-Earth Science and Technology, Atmosphere and Ocean Research Institute, and National Institute for Environmental Studies, Japan	MIROC3.2 Medres	MIROC-ESM-CHEM
Japan Agency for Marine-Earth Science and Technology, Atmosphere and Ocean Research Institute, and National Institute for Environmental Studies, Japan	MIROC3.2Hires	MIROC-ESM
Meteorological Research Institute		MIROC5
Japan Agency for Marine-Earth Science and Technology, Atmosphere and Ocean Research Institute, and National Institute for Environmental Studies, Japan	MRI-CGCM2	MRI-CGCM3
Max Planck Institute for Meteorology (MPI-M)		MPI-ESM-LR

used as a reference in interpreting the sc_PDSI_pm changes. However, we used the anomaly corresponding to the 20th or 10th percentile to define drought areas.

3 Model-simulated historical drought changes

Figure 1 compares the linear trends of annual sc_PDSI_pm during 1950–2014 calculated using observational data and the CMIP3 and CMIP5 multi-model all-forcing simulations. As pointed out by Dai (2013a), many of the regional change patterns in the observation-based sc_PDSI_pm (Fig. 1a) result from unforced, internal climate variations, such as the decadal to multi-decadal variations in surface temperature (T) and P associated with the Inter-decadal Pacific Oscillation (IPO) (Dai 2013b; Dai et al. 2015; Dong and Dai 2015). Since the internal variations are realization-dependent, i.e., their temporal evolution depends on the initial conditions of the real world and of the climate models, they are not comparable between individual realizations (such as the real world and individual model runs). On the other hand, the trends in the CMIP3 and CMIP5 ensemble mean
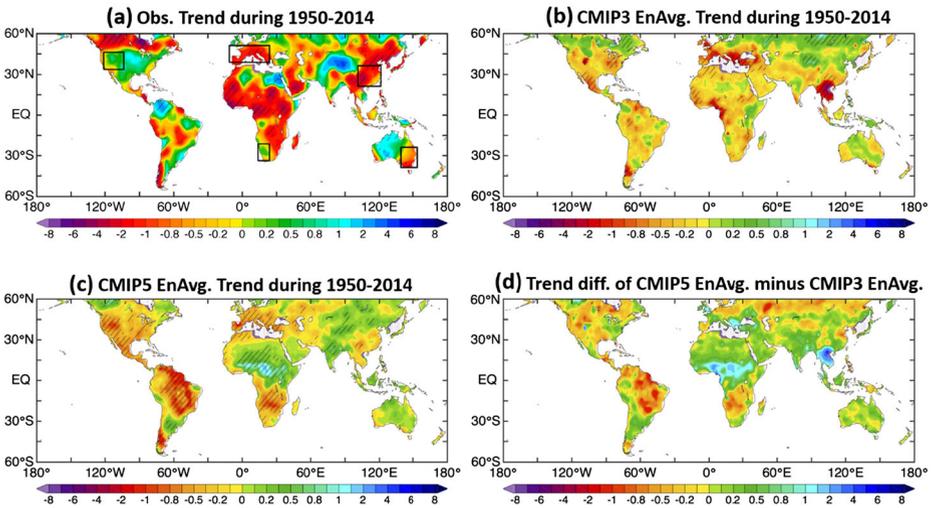
Fig. 1 Trend maps of annual sc_PDSI_pm (changes per 50 years) during 1950–2014 for (**a**) observation-based estimates, (**b**) CMIP3 ensemble mean, and (**c**) CMIP5 ensemble mean. (**d**) is the difference of annual sc_PDSI_pm trends between the CMIP5 and CMIP3 ensemble mean. The stippling indicates the trend or correlation is statistically significant at the 5 % level. The *rectangle boxes* in (**a**) are the five selected regions used in Figs. 5 and 6. The linear trend was estimated using the robustfit method, which considers the effects of outliers and end points (Street et al. 1988; see http://cn.mathworks.com/help/stats/robustfit.html)

(Fig. 1b-c) represent mostly forced changes caused by similar historical GHG and other forcing, thus they should be comparable.

With these in mind, Fig. 1 suggests that internal variability seems to dominate over the forced signal so far and causes larger trends than the model-simulated changes over many land areas, such as North America and parts of East Asia, while the drying over southern Europe, South Asia and parts of South America appears to be consistent with the model-simulated forced changes. Large differences between the CMIP5 and CMIP3 trends appear over central Africa (around 0–15° N), the Amazon, and parts of Southeast Asia and Southeast Europe (Fig. 1d). We examined the trend maps in individual models (not shown) and found large regional differences among the individual model runs for both the CMIP5 and CMIP3 models, presumably due to internal variability. Thus, we attribute the large regional differences shown in Fig. 1d primarily to the (uncorrelated) residual internal variations in the ensemble mean (due to the relatively small ensemble size of 12 for CMIP3 and 14 for CMIP5), with secondary contributions from different response patterns in CMIP3 and CMIP5 models. The key message from Fig. 1 is that regional drying trends so far are still dominated by internal climate variability and thus cannot be compared with model-simulated response to external climate forcing.

Despite the large regional difference, the leading modes of the sc_PDSI_pm from the observation-based estimate, and the CMIP3 and CMIP5 model simulations (Fig. 2) all show a global trend that represents drying over central Africa (except the CMIP5), southern Europe, and many parts of Asia and South America. The CMIP5 models show a large wetting trend over a zone around 8°–10° N that is absent in the CMIP3 models (Figs. 1b-c and 2b-c). In other words, the forced global-mean signal in sc_PDSI_pm may be detectable in the observation-based estimate, despite the large regional differences due to uncorrelated natural variations, as found previously by Dai (2013a).
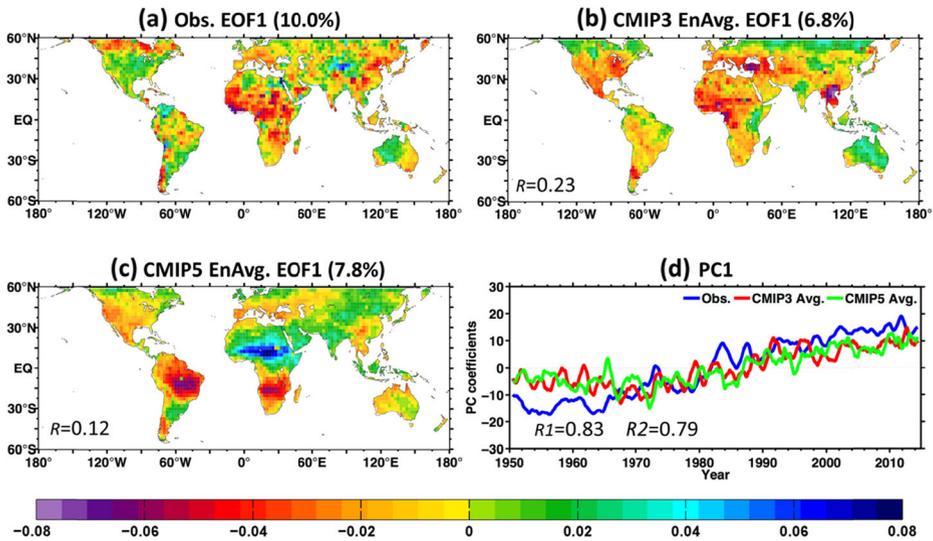
Fig. 2 The leading EOF of monthly sc_PDSI_pm anomalies from 1950 to 2014 (normalized by its standard deviation prior to the EOF analysis) for **(a)** observation-based estimates, **(b)** CMIP3 ensemble mean, **(c)** CMIP5 ensemble mean, and **(d)** their corresponding PC time series (13-point moving averaged). The explained percentage of the total variance is also shown on top of **(a)**–**(c)**. The pattern correlation (R) of the CMIP3 and CMIP5 EOF with **(a)** is also shown in **(b-c)**. In **(d)**, the PC correlation coefficient between the observation-based and the CMIP3 ($R1$) or CMIP5 ensemble ($R2$) is also shown. The high $R1$ and $R2$ values are mostly due to correlation of the trends

4 Model-projected future drought changes

4.1 Changes in drought frequency

Figure 3 shows that large increases in projected future precipitation in the CMIP5 models over 8°–10° N around the Sahel that is also evident in sc_PDSI_pm historical changes (Fig. 2) and their future projections (Fig. 4) based on the 14 CMIP5 models (Zhao and Dai 2015), while the precipitation (Fig. 3; IPCC 2007) and sc_PDSI_pm changes (Fig. 4) in the CMIP3 models over this region are more modest. However, when more CMIP5 models are included, the magnitude of this precipitation increase is significantly reduced (Fig. 3c).

Figures 4a-b show substantial decreases (i.e., drying) by 0.5 ~ 2 units in sc_PDSI_pm in the 21st century for both the CMIP3 and CMIP5 model projections over most of the Americas, Africa, Europe, Australia, and western and southeastern Asia. For comparison, conditions with PDSI ≤ −1 are considered drought by Palmer (1965). It is assuring that the CMIP3 and CMIP5 models show broadly consistent drying patterns. Nevertheless, noticeable differences are seen over the Sahel region and northwestern Australia, both are related to the differences in the projected precipitation changes, which are quite uncertain over these two regions (Fig. 3; IPCC 2007, 2013). Several regions, including East Africa, India, central and northern Asia, show considerable increases (i.e., wetting) in the sc_PDSI_pm due to large precipitation increases over these regions (Figs. 3 and 4).

The sc_PDSI_pm increases over East Africa is especially large and in sharp contrast to the large decreases over the rest of Africa, and it is also in contrast to recent drought conditions
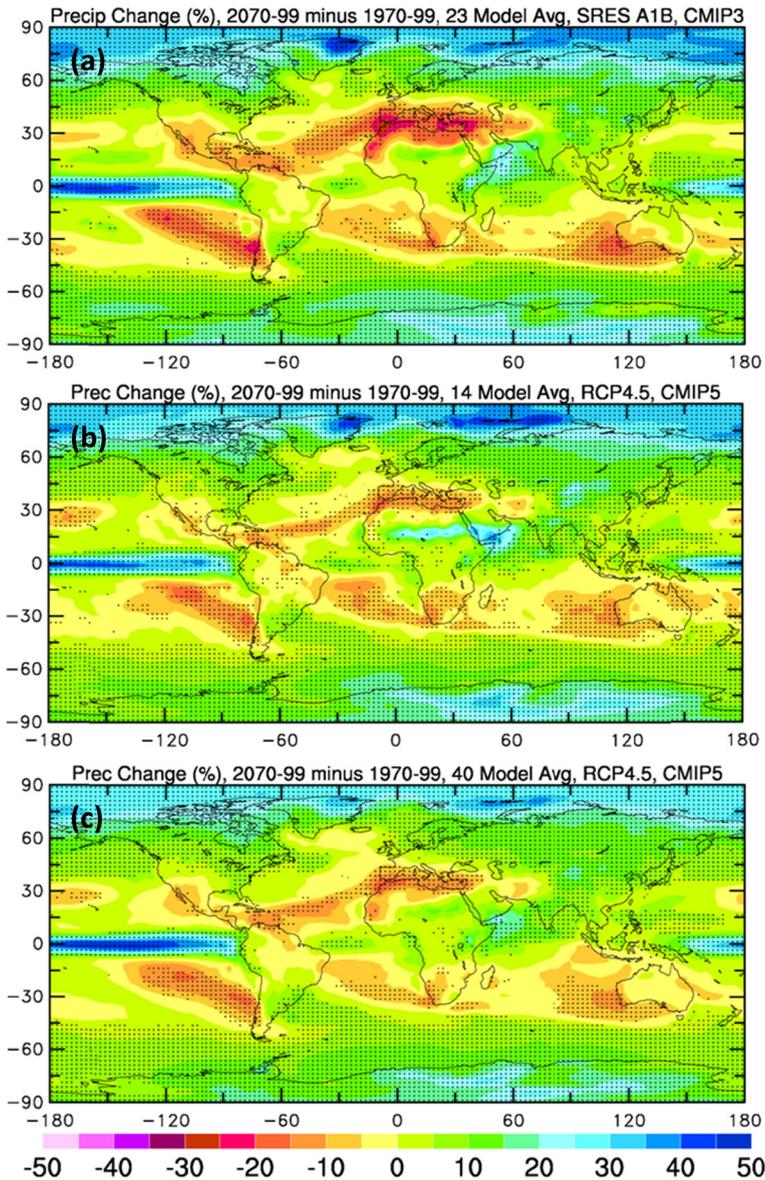
Fig. 3 Percentage change in annual precipitation from 1970 to 1999 to 2070–2099 simulated by (**a**) 23 CMIP3 models under the moderate SRES A1B scenario, (**b**) 14 and (**c**) 40 CMIP5 models under the low-moderate RCP4.5 scenario. Stippling indicates at least 80 % of the models agree on the sign of change. See http://cmip-pcmdi.llnl.gov/ for a list of the CMIP models

over East Africa (Rowell et al. 2015). The precipitation increase over East Africa appears to be part of a large zone with increasing rainfall (Fig. 3) associated with enhanced moist convection in the inter-tropical convergence zone (ITCZ) from Africa to the Indian Ocean in both CMIP models. However, this zone of increasing precipitation shows a larger response than the CMIP3 models over a narrow band centered at 16°N in North Africa in the 14 CMIP5 models
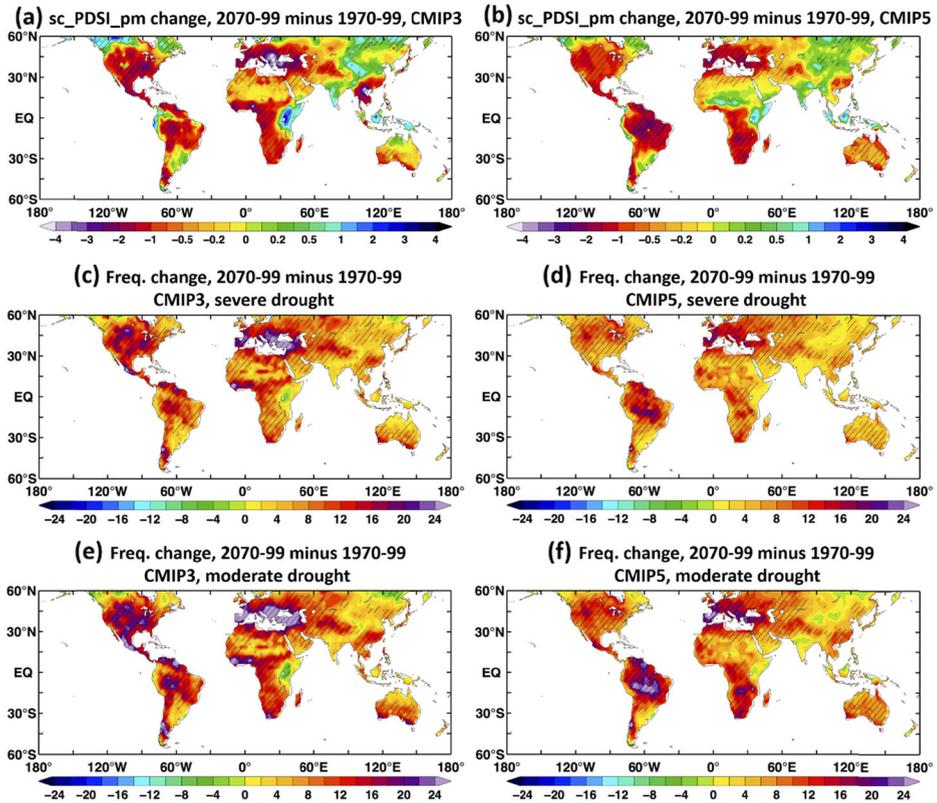
Fig. 4 Long-term changes from 1970 to 1999 to 2070–2099 over land in annual sc_PDSI_pm from **(a)** 12 CMIP3 models under the A1B scenario and **(b)** 14 CMIP5 models under the RCP4.5 scenario. Also shown are the multi-model ensemble averaged changes of drought frequency (defined as the percentage of the time in drought conditions, not percentage changes) from 1970 to 1999 to 2070–2099, with drought being defined locally as months below the 10th for **(c)** and **(d)**, and 20th for **(e)** and **(f)** percentile of the 1970–1999 period based on monthly sc_PDSI_pm anomalies (relative to 1970–1999 mean) from the CMIP3 for **(c)** and **(e)**, and CMIP5 for **(d)** and **(f)**. The stippling indicates at least 80 % of the models agree on the sign of change

used for the sc_PDSI_pm calculations (but not in the 40 CMIP5 models) (Fig. 3). Thus, while there are large uncertainties for the projected precipitation increases for the zone around 16° N, the rainfall (and thus sc_PDSI_pm) increases in East Africa appear to be a robust response seen in both CMIP3 and CMIP5 models associated with intensified convection in the ITCZ over the Indian Ocean sector. However, the reliability of the CMIP5 model-simulated East African rainfall has been questioned due to its poor seasonal cycle (Yang et al. 2014).

Following Zhao and Dai (2015), we define drought events as periods with sc_PDSI_pm anomalies (relative to 1970–1999 mean) below the value corresponding to the 20th (moderate to severe drought) or 10th (severe drought) percentile of the current (1970–1999) climate at each grid box. Consistent with the CMIP5 results shown by Zhao and Dai (2015), the spatial patterns of the change in drought frequency are comparable for the two types of drought. The frequency increase of the severe drought is only slightly lower than that of the moderate-to-severe drought, which means that in relative terms the severe drought frequency increases nearly twice as faster as the moderate-to-severe drought in both the CMIP3 and CMIP5 projections (Fig. 4c–f). Increased drought frequency is seen over nearly all land areas, and

the increase is especially large (by 8–24 % of the time) over most of southern Europe, the Americas and Africa (except East Africa).

The CMIP5 models project larger increases in drought frequency over Australia than the CMIP3 models, especially over its Northwest, mainly due to the differences in the projected precipitation changes over northern and central Australia (Fig. 3). The precipitation change over Australia appears to be part of a large drying zone in the Southern Hemisphere that originates from the subtropics and has a slightly different shape in the CMIP3 and CMIP5 models (Fig. 3). Thus, the overall drying over Australia is likely to be a robust response related to the large-scale subtropical drying, but the exact northern boundary of this drying zone differs in the CMIP3 and CMIP5 models and this affects the projected rainfall (and thus drought) changes over northern Australia.

The drought frequency changes are more widespread than the decreases in the mean sc_PDSI_pm, as many areas with increasing sc_PDSI_pm also show increased drought frequency (Fig. 4). These contrasting changes in the mean sc_PDSI_pm and its extremes (i.e., drought) can be explained by the flattening of its probability density functions (PDFs) discussed below.

4.2 Changes in the PDFs of the sc_PDSI_pm

Figure 5 shows the estimated PDFs from the multi-model averaged, smoothed histograms of monthly sc_PDSI_pm anomalies (relative to 1970–1999 mean) from all grid boxes over global land between 60° S and 60° N and five regions outlined in Fig. 1a for the current (1970–1999) and future (2070–2099) periods. For comparison, the PDFs of our observation-based sc_PDSI_pm are also shown for the current period. It is clear that the sc_PDSI_pm anomalies largely follow the Gaussian distributions, especially when averaged over the global land (as expected from the central limit theorem). The shapes of the model-simulated PDFs are similar with the observation-based estimates especially for Australia, but with larger variances and lower peaks especially over southeast Asia and Europe (Fig. 5).

A major change in the future PDFs for both the CMIP3 and CMIP5 projections is the flattening that is characterized by a reduced peak and increased spread during 2070–2099 compared with 1970–1999, besides the mean shift to the left (i.e., drying) for all the regions shown in Fig. 5, especially for the western United States and Europe. As shown in Zhao and Dai (2015), the PDF flattening is also seen in the CMIP5 projected soil moisture content and runoff, essentially over all land areas and especially in the Northern Hemisphere.

As shown previously (e.g., Zhao and Dai 2015), a small shift of the mean to the left can lead to a large increase in the frequency of drought (the extreme values on the left tail). The flattening of the projected PDFs further enhances future drought frequency over most land areas, especially in the western United States, Europe and other Northern Hemisphere land areas. The flattening is slightly more severe in the CMIP3 projections than the CMIP5 simulations, likely due in part to the slightly higher A1B emissions forcing in the CMIP3 than the RCP4.5 scenario for the CMIP5 models.

4.3 Changes in drought areas

Zhao and Dai (2015) showed that global area under the moderate (severe) drought conditions could increase from 20 % to about 28 % (from 10 % to 16 %) by 2080–2099 based on the
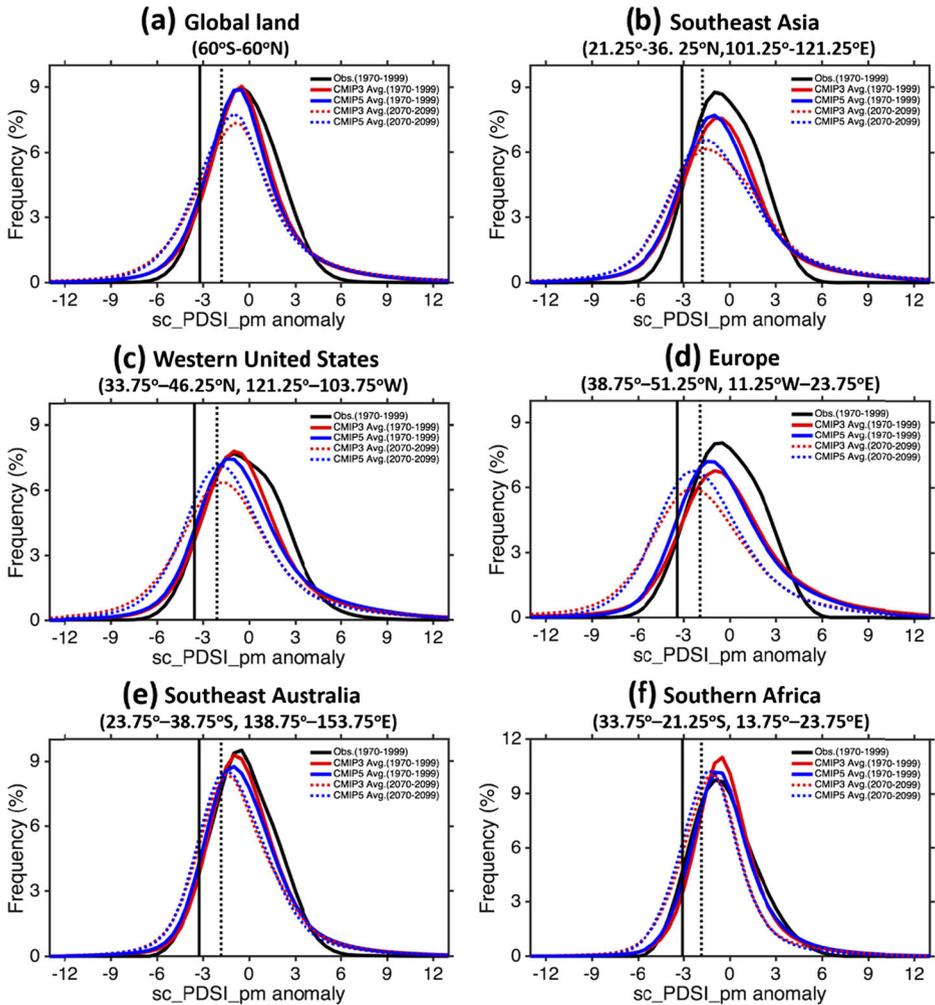
Fig. 5 The probability density functions (PDFs) of the monthly sc_PDSI_pm anomalies (relative to 1970–1999 mean) for all the grid boxes over the global (60 °S-60 °N) and five select land regions outlined in Fig. 1a, derived using cubic spline fitting from smoothed histograms during 1970–1999 (*solid lines*) and 2070–2099 (*dashed lines*). The *black line* is for the observation-based sc_PDSI_pm, while the colored lines are for the 12 CMIP3 (*red*) and 14 CMIP5 (*blue*) model ensemble mean. The *vertical solid* and *dashed black lines* indicate the 10th and 20th percentiles, respectively, of the observation-based sc_PDSI_pm during 1979–1999

CMIP5 projections under the RCP4.5 scenario. Here, we compare the drought area changes from both the CMIP3 and CMIP5 multi-model simulations from 1900 to 2099 together with their inter-model spreads for the globe, the Northern and Southern Hemisphere. Figure 6 shows that the long-term changes derived from the CMIP3 multi-model simulations are consistent with the CMIP5 results, except for slightly larger drought areas for the globe and Northern Hemisphere after about the 2060s for the CMIP3, as the RCP4.5 forcing stabilizes after 2065 in the CMIP5 (Van Vuuren et al. 2011). The CMIP3 models also show a larger spread than the CMIP5 models for the global and Northern Hemisphere drought areas after about the 2050s (Fig. 6a, c).
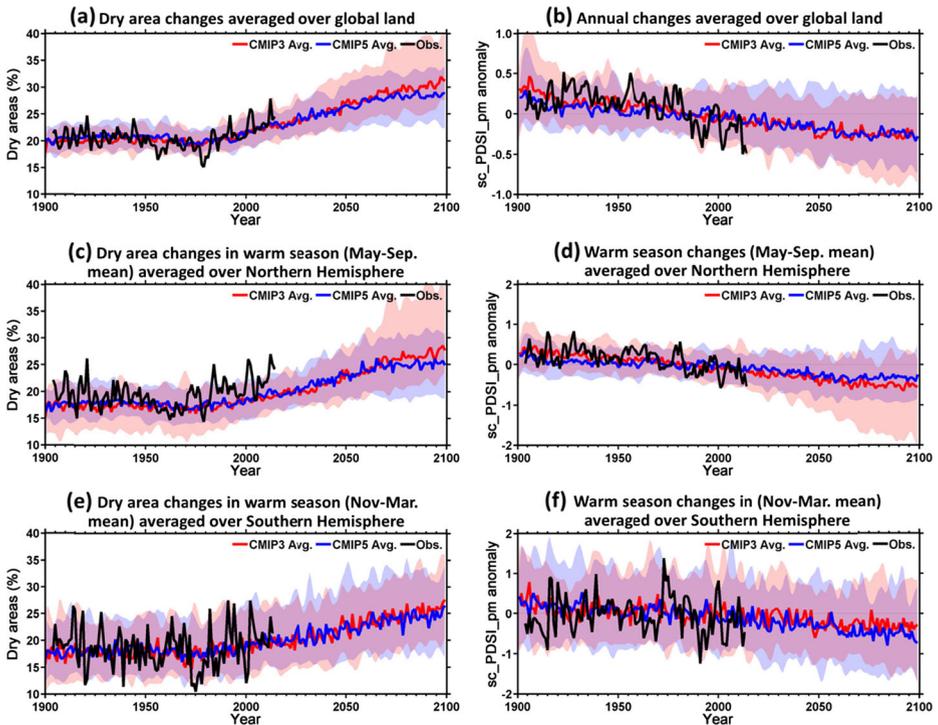
Fig. 6 Left column: Multi-model ensemble-mean time series of the drought areas (in percentage of the total land area between 60 °S and 60 °N) with the drought defined locally with monthly sc_PDSI_pm anomalies (relative to 1970–1999 mean) below the 20th percentile of the 1970–1999 period. Three cases are shown: the observation-based estimate (*black*), the CMIP3 (*red*) and CMIP5 (*green*) ensemble mean over **(a)** global land (60 °S-60 °N) for all months, **(c)** the warm season from May to September over Northern Hemisphere land, and **(e)** the warm season from November to March over Southern Hemisphere land. Right column: Same as the left column but for the mean sc_PDSI_pm changes. The pink (*light blue*) areas are the spreads (i.e., the minimum to maximum range of the models) of the CMIP3 (CMIP5) models. The overlying spread range of the CMIP3 and CMIP5 models is in *magenta color*

The warm-season drought changes (Fig. 6c–f) are similar to the all-season changes (Fig. 6a-b), and they are also comparable between the CMIP3 and CMIP5 simulations, except for the Northern Hemisphere after the 2060s as noticed above. The large ensemble range shown in Fig. 6 primarily reflects the internal climate variability (plus some inter-model uncertainties), while the ensemble mean shows mostly the forced response to external GHG and other forcing. Overall, the global area under moderate drought conditions could increase from about 20 % to 33 % in the CMIP3 simulations from the 1990s to the 2090s, which is about 5 % more than that in the CMIP5 simulations. We also conducted a similar analysis for global areas under the severe drought (<10th percentile) conditions and found the increase in the drought area is also about 5 % more in the CMIP3 simulations (from 10 to 20 %) than the CMIP5 projections (from 10 to 16 %) by the 2090s. The CMIP3 models produce slightly larger changes after about the 2060s mainly due to the slightly higher A1B emissions in the CMIP3 models than the RCP4.5 scenario for the CMIP5 models.

Figure 6 shows that as an individual realization, the observation-based estimate (black line) exhibits, as expected, much larger variations than the multi-model ensemble mean, but they are

generally within the model ensemble spread. Furthermore, long-term variations and changes in the drought areas and the mean sc_PDSI_pm from 1900 to 2014 are largely consistent between the observation-based estimate and the model simulations. This is particularly true for the global drought areas (Fig. 6a). Thus, the observation-based estimates of global and hemispheric drought changes since 1900 are consistent with the CMIP3 and CMIP5 model-simulated response to historical GHG and other external forcing, while the short-term variations are within the model spread of the internal variability.

5 Summary

In part II of this study, we first compared historical agricultural drought changes (i.e., sc_PDSI_pm) and the leading modes of variability from 1950 to 2014 simulated by the CMIP3 and CMIP5 models with the observation-based estimates, and then examined the projected changes in the mean sc_PDSI_pm, its PDFs, and drought frequency and areas from the CMIP3 and CMIP5 model simulations for the 21st century under the moderate A1B (for CMIP3) and low-moderate RCP4.5 (for CMIP5) scenarios. The main findings are summarized as follows.

1) During 1950–2014, both the CMIP3 and CMIP5 multi-model ensemble means, which represent mostly forced changes, do not match well the regional trend patterns in the observation-based sc_PDSI_pm over many land areas. This suggests that regional drought trends are still dominated by internal climate variability and thus not detectable yet, which confirms the finding of Dai (2013a).

2) However, long-term changes in global and hemispheric drought areas and mean sc_PDSI_pm from 1900 to 2014, especially since 1950, are broadly consistent with the CMIP3 and CMIP5 model-simulated response to historical GHG and other external forcing (again consistent with Dai 2013a), while the short-term variations are within the model-simulated spread of internal variability.

3) Based on the sc_PDSI_pm, both the CMIP3 and CMIP5 models project continued increases by 0.5–2 unit (50–200 % in a relative sense) in the 21st century in global drought frequency and area even under low-moderate emissions scenarios. The drought increases result firstly from a mean shift (toward drier conditions) and secondarily from a flattening of the PDFs of the sc_PDSI_pm. This flattening is especially pronounced over the Northern Hemisphere land, leading to increased drought frequency even over areas with increasing sc_PDSI_pm.

4) Increases in precipitation and sc_PDSI_pm (i.e., wetting) during the 21st century over East Africa are seen in both the CMIP3 and CMIP5 model projections, and they are part of a large zone of increasing precipitation associated with the ITCZ in the African and Indian Ocean sector, although CMIP5 model-simulated East African rainfall has a poor seasonal cycle and thus may be less reliable (Yang et al. 2014).

5) Some disagreements exist in the precipitation and sc_PDSI_pm changes over a zone centered about 16° N in North Africa and over northern Australia between the CMIP3 and CMIP5 model-simulated responses to increased GHGs. The disagreements result from the different responses of the African ITCZ and the dry zone over Australia in the two generations of models.

6) As shown in Zhao and Dai (2015), the decrease in sc_PDSI_pm is caused by warming-induced ubiquitous PET increase and reduction in subtropical land precipitation.

However, the exact cause of the PDF flattening is unknown and requires further investigation.

References

Burke EJ, Brown SJ (2008) Evaluating uncertainties in the projection of future drought. J Hydrometeorol 9:292–299. doi:10.1175/2007JHM929.1

Burke EJ, Brown SJ, Christidis N (2006) Modeling the recent evolution of global drought and projections for the twenty-first century with the hadley centre climate model. J Hydrometeorol 7:1113–1125

Cook BI, Smerdon JE, Seager R, Coats S (2014) Global warming and 21st century drying. Clim Dyn 43:2607–2627

Cook BI, Ault TR, Smerdon JE (2015) Unprecedented 21st-century drought risk in the American Southwest and Central Plains. Sci Avd 1:e1400082

Dai A (2011a) Characteristics and trends in various forms of the palmer drought severity index during 1900–2008. J Geophys Res 116:D12115

Dai A (2011b) Drought under global warming: a review. WIREs Clim Change 2:45–65

Dai A (2013a) Increasing drought under global warming in observations and models. Nat Clim Chang 3:52–58

Dai A (2013b) The influence of the inter-decadal Pacific Oscillation on U.S. precipitation during 1923–2010. Clim Dyn 41:633–646

Dai A, Zhao T (2016) Uncertainties in historical changes and future projections of Drought. Part I: Uncertainties in estimating historical drought changes. Clim Chang. doi:10.1007/s10584-016-1705-2

Dai A, Trenberth KE, Karl TR (1998) Global variations in droughts and wet spells: 1900–1995. Geophys Res Lett 25:3367–3370. doi:10.1029/98GL52511

Dai A, Trenberth KE, Qian T (2004) A global dataset of palmer drought severity index for 1870–2002: relationship with soil moisture and effects of surface warming. J Hydrometeorol 5:1117–1130. doi:10.1175/JHM-386.1

Dai A, Fyfe JC, Xie S-P, Dai X (2015) Decadal modulation of global surface temperature by internal climate variability. Nat Clim Chang 5:555–559. doi:10.1038/nclimate2605

Dong B, Dai A (2015) The influence of the Inter-decadal Pacific Oscillation on temperature and precipitation over the globe. Clim Dyn 45:2667–2681. doi:10.1007/s00382-012-1446-5

Hobbins MT, Dai A, Roderick ML, Farquhar GD (2008) Revisiting potential evapotranspiration parameterizations as drivers of long-term water balance trends. Geophys Res Lett 35:L12403. doi:10.1029/2008GL033840

IPCC (2007) In: Solomon S et al. (eds) Climate Change 2007: the physical science basis. Cambridge University Press, Cambridge

IPCC (2013) In: TE S et al. (eds) Climate Change 2013: the physical science basis. Cambridge University Press, Cambridge

Meehl GA, Stocker TF, Collins WD, Friedlingstein P, Gaye AT, et al. (2007) In: Solomon S et al. (eds) Global Climate Projections. Climate Change 2007: The physical science basis. contribution of working group I to the fourth assessment report of the IPCC. Cambridge University Press, Cambridge, UK and New York, NY, pp. 746–845

Palmer WC (1965) Meteorological drought. US Weather Bureau Research Paper 45: 55 pp

Prudhomme C et al. (2014) Hydrological droughts in the 21st century, hotspots and uncertainties from a global multimodel ensemble experiment. Proc Natl Acad Sci U S A 111:3262–3267. doi:10.1073/pnas.1222473110

Rind D, Goldberg R, Hansen J, Rosenzweig C, Ruedy R (1990) Potential evapotranspiration and the likelihood of future drought. J Geophys Res 95:9983–10004

Rowell D, Booth B, Nicholson S, Good P (2015) Reconciling past and future rainfall trends over East Africa. J Clim 28(24):9768–9788. doi:10.1175/JCLI-D-15-0140.1

Sheffield J, Wood EF (2008) Projected changes in drought occurrence under future global warming from multi-model, multi-scenario, IPCC AR4 simulations. Clim Dyn 31:79–105

Sheffield J, Wood EF, Roderick ML (2012) Little change in global drought over the past 60 years. Nature 491(7424):435–438. doi:10.1038/nature11575

Street JO, Carroll RJ, Ruppert D (1988) A note on computing robust regression estimates via iteratively reweighted least squares. Am Stat 42:152–154

Taylor KE, Stouffer RJ, Meehl GA (2012) An overview of CMIP5 and the experiment design. Bull Am Meteorol Soc 93:485–498

Taylor IH, Burke E, McColl L, Falloon PD, Harris GR, McNeall D (2013) The impact of climate mitigation on projections of future drought. Hydrol Earth Syst Sci 17:2339–2358. doi:10.5194/hess-17-2339-2013

Trenberth KE, Dai A, van der Schrier G, Jones PD, Barichivich J, Briffa KR, Sheffield J (2014) Global warming and changes in drought. Nat Clim Chang 4:17–22

van der Schrier G, Efthymiadis D, Briffa KR, Jones PD (2007) European Alpine moisture variability for 1800–2003. Int J Climatol 27:415–427. doi:10.1002/joc.1411

van der Schrier G, Jones PD, Briffa KR (2011) The sensitivity of the PDSI to the Thornthwaite and Penman-Monteith parameterizations for potential evapotranspiration. J Geophys Res Atmos 116:D03106. doi:10.1029/2010JD015001

van der Schrier G, Barichivich J, Briffa KR, Jones PD (2013) A scPDSI-based global data set of dry and wet spells for 1901–2009. J Geophys Res Atmos 118:4025–4048. doi:10.1002/jgrd.50355

van Vuuren DP et al. (2011) The representative concentration pathways: an overview. Clim Dyn 109:5–31

Wang GL (2005) Agricultural drought in a future climate: results from 15 global climate models participating in the IPCC 4th assessment. Clim Dyn 25:739–753

Wehner M, Easterling DR, Lawrimore JH, Heim RR, Vose RS, Santer BD (2011) Projections of future drought in the continental United States and Mexico. J Hydrometeorol 12:1359–1377

Wells N, Goddard S, Hayes MJ (2004) A self-calibrating Palmer drought severity index. J Clim 17:2335–2351

Yang W, Seager R, Cane MA, Bradfield Lyon B (2014) The East African long rains in observations and models. J Clim 27:7185–7202. doi:10.1175/JCLI-D-13-00447.1

Zhai J, Su B, Krysanova V, Vetter T, Gao C, Jiang T (2010) Spatial variation and trends in PDSI and SPI indices and their relation to streamflow in 10 large regions of China. J Clim 23:649–663. doi:10.1175/2009JCLI2968.1

Zhao T, Dai A (2015) The magnitude and causes of global drought changes in the 21st century under a low–moderate emissions scenario. J Clim 28:4490–4512